Computers & Structures Vol. 25, No. 2, pp. 211–224, 1987
Printed in Great Britain.

0045-7949/87 $3.00 + 0.00

COMPUTATION OF POST-BIFURCATION AND POST-FAILURE BEHAVIOR OF STRAIN-SOFTENING SOLIDS

R. DE BORST
TNO Institute for Building Materials and Structures, Software Engineering Department, P.O. Box 49, 2600 AA Delft, The Netherlands

(*Received* 13 *May* 1986)

Abstract—Consequences of the use of strain-softening models are reviewed both theoretically and numerically. A most serious consequence of strain-softening is that it may cause snap-back behavior on a structural level. This is demonstrated by means of two concrete structures, a reinforced concrete structure and an unreinforced specimen. In order to simulate the highly localized failure mode in a strain-softening solid, it appeared necessary to modify the arc-length method. The paper furthermore demonstrates that bifurcation points which occur in strain-softening solids can be located by numerical methods and that the post-bifurcation response can be traced successfully.

1. INTRODUCTION

Strain-softening is an unpleasant phenomenon displayed by materials like concrete and geomaterials (soils, rock). It hampers finite element applications as calculations are repeatedly reported to be unstable and as the analyst often finds it difficult to obtain a truly converged solution.

Another major difficulty in applying finite element models to strain-softening materials is the fact that the results are not objective with regard to mesh refinement, i.e. the results do not converge to the "true" solution when the finite element mesh is refined [3, 4]. To remedy this disease, it has been proposed to make the softening modulus a function of the element size. In doing so, objective results can again be obtained [4, 22, 26, 31].

Starting from a somewhat different point of view, Crisfield [12] arrived at similar conclusions. He also demonstrated by the simple example of a bar loaded in pure tension that solutions in the strain-softening regime are non-unique, and moreover, that some equilibrium branches emanating from the bifurcation point lead to snap-back behavior. These observations have severe consequences for analyzing concrete structures, either reinforced or not. It implies for instance that truly converged solutions may not always be obtained by customary displacement control, but that we often have to resort to more sophisticated techniques like "arc-length" control in order to obtain a proper solution [6, 11, 24, 25]. Here, it even appears that the traditional "arc-length" in the n-dimensional displacement space is not very well suited for controlling the solution process in strain-softening solids. Indeed, the author has found that a global constraint equation which involves all degrees of freedom cannot be employed successfully to obtain converged solutions when analyzing concrete structures [8, 9]. Use of only a few dominant degrees of freedom or removal of a number of degrees of freedom from the constraint equation resulted in a major improvement in convergence characteristics. The failure of a global norm of displacement increments may be explained by considering that for problems involving softening, failure or bifurcation modes are often highly localized. Hence, only a few nodes contribute to the norm of displacement increments and failure is not sensed accurately by a global norm.

To gain perspective we will start this article by reviewing the pioneering work of Crisfield [12] in some detail. After that, we will outline a numerical approach to detect bifurcation points and to trace post-bifurcation and post-failure paths in strain-softening solids. The procedures are subsequently applied to a numerical bifurcation analysis of a bar loaded in tension, and to two limit problems involving snap-back behavior, whereby it is noted that in the latter case the snap-behavior is believed to be physical and does not have a numerical cause as was probably the case in some previous analyses [13, 14].

2. STRAIN-SOFTENING, NON-UNIQUENESS AND SNAP-BACK BEHAVIOR

We consider an unreinforced bar which is subjected to pure tension [12] and the material of the bar is modeled as elastic-softening with an ultimate strain ϵ_u at which the tensile strength has vanished completely (see Fig. 1). ϵ_u is assumed to be equal to n times the strain at the tensile strength (ϵ_e). The bar is modeled with m elements (see Fig. 2). If we have a perfect bar, so that all elements have exactly the same tensile strength and so on, the bar deforms uniformly throughout the loading process and the load–deflection curve is simply a copy of the imposed

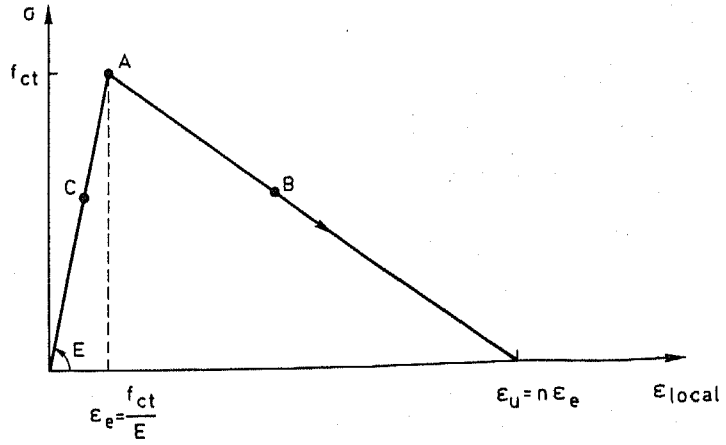

Fig. 1. Stress–strain law for concrete in tension. The stress is plotted against the total strain, i.e. the sum of crack strain and concrete strain.

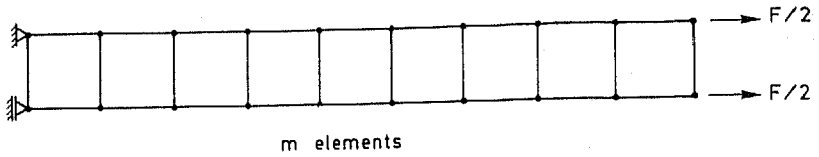

Fig. 2. Model of bar composed of strain-softening material.

stress–strain law. However, if one element has a slight imperfection, only this element will show loading while the other elements will show unloading. In this situation, the imposed stress–strain law at local level is not reproduced. Instead, an average strain is calculated in the post-peak regime which is smaller than the strain of the stress–strain law. This may be explained as follows. The element which shows loading will follow the path A–B in Fig. 1, while the other elements will follow the path A–C. This implies that when all elements have the same dimensions, we have for the average strain increment $\Delta\bar{\varepsilon}$

$$\Delta\bar{\varepsilon} = \frac{1}{m}\left[-(m-1)\frac{\Delta\sigma}{E} + \frac{\Delta\sigma}{E/(n-1)}\right] = \left[\frac{n}{m} - 1\right]\frac{\Delta\sigma}{E}. \quad (1)$$

Consequently, when we increase the number of elements while keeping the length of the bar fixed, the average strain in the post-peak regime gradually becomes smaller and for $m > n$ the average strain in the post peak regime even becomes smaller than the strain at peak load (Fig. 3). This implies that for $m > n$, the load–deflection curve shows a "snap-back" [12]. It is noted that similar results have also been derived for beams composed of strain-softening material [29].

The above results imply that computational results for materials with a local softening constitutive law are not objective upon mesh refinement. To remedy this disease, it has been proposed to make the softening modulus dependent on the element size [4, 20]. Numerical experiments have confirmed that numerical results are then objective with regard to mesh refinement [4, 22, 26, 31]. The problem of making the softening modulus dependent on the element size is that, for an arbitrary concrete structure, the spread of the softening region is not known in advance. Consequently, the observation that use of a local softening law may involve snap-back behavior on structural level may hold even when we use a model in which the softening modulus has been adapted to some structural size.

3. COMPUTATIONAL TECHNIQUES

In spite of its apparent simplicity the example of a bar loaded in tension is a challenging problem for a numerical simulation. To achieve this goal, current numerical techniques must either be modified or be employed very judiciously. First, we must have a criterion to detect a bifurcation point in a discrete mechanical model. In the present case, the bifurcation point is obvious as it simply coincides with the limit point, but this seldom happens. In general, bifurcation will be possible when the lowest eigenvalue vanishes [19]. In numerical applications, the lowest eigenvalue will never become exactly zero owing to round-off errors. Therefore, it has been assumed that bifurcation is possible when the lowest eigenvalue becomes slightly negative. It is noted in passing that the above statement holds rigorously for mechanical systems with a symmetric stiffness matrix,

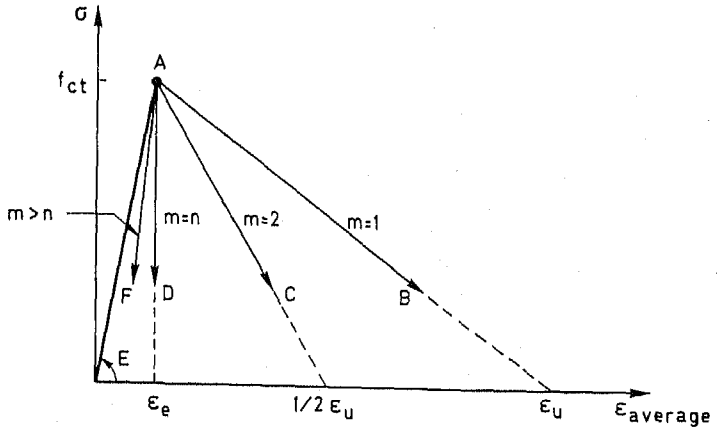

Fig. 3. Possible post-bifurcation behavior for a bar loaded in tension. Which equilibrium path is followed depends on the number of elements in which the crack localizes.

but that for systems with a non-symmetric stiffness matrix the situation is less clear-cut [9].

Having determined the bifurcation point by an eigenvalue analysis of the tangent stiffness matrix, continuation on the localization branch instead of on the fundamental branch can be forced by adding a part of the eigenmode $\mathbf{v}_1$, which belongs to the vanishing eigenvalue, to the incremental displacement field of the fundamental path $\Delta\mathbf{a}^*$ [9, 25]:

$$\Delta\mathbf{a} = \alpha(\Delta\mathbf{a}^* + \beta\mathbf{v}_1), \tag{2}$$

with α and β scalars. The magnitude of these scalars is fixed by second-order terms or by switch conditions for elastoplasticity or for plastic-fracturing materials. The most simple way to determine β numerically is to construct a trial displacement increment $\Delta\mathbf{a}$ such that it is orthogonal to the fundamental path:

$$\Delta\mathbf{a}^T\Delta\mathbf{a}^* = 0, \tag{3}$$

where the symbol T is employed to denote a transpose. Substituting equation (2) in this expression yields, for β,

$$\beta = -\frac{(\Delta\mathbf{a}^*)^T\Delta\mathbf{a}^*}{(\Delta\mathbf{a}^*)^T\mathbf{v}_1}, \tag{4}$$

so that we obtain for $\Delta\mathbf{a}$

$$\Delta\mathbf{a} = \alpha\left\{\Delta\mathbf{a}^* - \frac{(\Delta\mathbf{a}^*)^T\Delta\mathbf{a}^*}{(\Delta\mathbf{a}^*)^T\mathbf{v}_1}\mathbf{v}_1\right\}. \tag{5}$$

Equation (5) fails when $(\Delta\mathbf{a}^*)^T\mathbf{v}_1 = 0$, i.e. when the bifurcation mode is orthogonal to the basic path. A simple remedy is to normalize $\Delta\mathbf{a}$ such that

$$(\Delta\mathbf{a}^*)^T\Delta\mathbf{a}^* = \Delta\mathbf{a}^T\Delta\mathbf{a}. \tag{6}$$

This results in:

$$\Delta\mathbf{a} = \frac{1}{\sqrt{(\Delta\mathbf{a}^*)^T\Delta\mathbf{a}^* - [(\Delta\mathbf{a}^*)^T\mathbf{v}_1]^2}} \times\left\{(\Delta\mathbf{a}^*)^T\mathbf{v}_1\Delta\mathbf{a}^* - (\Delta\mathbf{a}^*)^T\Delta\mathbf{a}^*\mathbf{v}_1\right\}. \tag{7}$$

The denominator of this expression never vanishes, since this would imply that the eigenmode is identical with the fundamental path.

In general, the bifurcation path will not be orthogonal to the fundamental path, but when we add equilibrium iterations, the orthogonality condition (3) will maximize the possibility that we converge on a bifurcation branch and not on the fundamental path, although this is not necessarily the lowest bifurcation path when more equilibrium branches emanate from the bifurcation point. When we do not converge on the lowest bifurcation path, this will be revealed by negative eigenvalues of the bifurcated solution. The above described procedure can then be repeated until we ultimately arrive at the lowest bifurcation path.

The procedure described above is well suited for assessing post-bifurcation behavior. Bifurcations, however, are rather rare in normal structures owing to imperfections, and even if a bifurcation point exists in a structure, numerical round-off errors and spatial discretization usually transfer the bifurcation point into a limit point unless we have a homogeneous stress field. This observation does not render the approach to bifurcation problems worthless as it provides a thorough insight which is of importance for the associated limit problems, but it is obvious that numerical procedures must also be capable of locating limit points and tracing post-limit behavior.

To control the incremental-iterative solution procedure, we have analogous to experiments load control and (direct) displacement control. However, either of these procedures may fail in particular circumstances. With load control, we are not able to overcome limit points at all, and with direct displacement control it is not possible to properly analyze snap-back behavior (see e.g. Fig. 3). Fortunately, a very general and powerful method has been developed within the realm of geometrically non-linear analysis. In this method, the incremental-iterative process is controlled indirectly using a norm of

incremental displacements [6, 11, 24, 25]. For this reason, the name "arc-length method" has been coined for the procedure. For materially non-linear analysis, a global norm on incremental displacements is often less successful due to localization effects and it may be more efficient to employ only one dominant degree of freedom or to omit some degrees of freedom from the norm of incremental displacements. The name arc-length control then no longer seems very appropriate. Instead we will use the term indirect displacement control.

In a nonlinear finite element analysis, the load is applied in a number of small increments (e.g. Bathe [2]). Within each load increment, equilibrium iterations are applied and the iterative improvement $\delta \mathbf{a}_i$ in iteration number i to the displacement increment $\Delta \mathbf{a}_{i-1}$ is given by

$$\delta \mathbf{a}_i = \boldsymbol{K}_{i-1}^{-1}[\boldsymbol{p}_{i-1} + \Delta\mu_i \boldsymbol{q}^*], \tag{8}$$

where $\boldsymbol{K}_{i-1}$ is the possibly updated stiffness matrix, $\boldsymbol{q}^*$ is a normalized load vector, $\Delta\mu_i$ is the value of the load increment which may change from iteration to iteration and $\boldsymbol{p}_{i-1}$ is defined by

$$\boldsymbol{p}_{i-1} = \mu_0 \boldsymbol{q}^* - \int_V \boldsymbol{B}^T \boldsymbol{\sigma}_{i-1} \, \mathrm{d}V. \tag{9}$$

In eqn (9) the symbols μ_0, $\boldsymbol{B}$ and $\boldsymbol{\sigma}_{i-1}$ have been introduced for, respectively, the value of the scalar load parameter at the beginning of the current increment, the strain-nodal displacement matrix and the stress vector at iteration number $i-1$.

The essence of controlling the iterative solution procedure indirectly by displacements is that $\delta \mathbf{a}_i$ is conceived to be composed of two contributions:

$$\delta \mathbf{a}_i = \delta \mathbf{a}_i^{\mathrm{I}} + \Delta\mu_i \delta \mathbf{a}_i^{\mathrm{II}} \tag{10}$$

with

$$\delta \mathbf{a}_i^{\mathrm{I}} = \boldsymbol{K}_{i-1}^{-1} \boldsymbol{p}_{i-1} \tag{11}$$

and

$$\delta \mathbf{a}_i^{\mathrm{II}} = \boldsymbol{K}_{i-1}^{-1} \boldsymbol{q}^*. \tag{12}$$

After calculating the displacement vectors $\delta \mathbf{a}_i^{\mathrm{I}}$ and $\delta \mathbf{a}_i^{\mathrm{II}}$, the value for $\Delta\mu_i$ is determined from some constraint equation on the displacement increments and $\Delta \mathbf{a}_i$ is subsequently calculated from

$$\Delta \mathbf{a}_i = \Delta \mathbf{a}_{i-1} + \delta \mathbf{a}_i. \tag{13}$$

Crisfield [11], for instance, uses the norm of the incremental displacements as constraint equation

$$\Delta \mathbf{a}_i^T \Delta \mathbf{a}_i = \Delta l^2, \tag{14}$$

where Δl is the arc-length of the equilibrium path in the n-dimensional displacement space. The drawback of this so-called spherical arc-length method is that it yields a quadratic equation for the load increment. To circumvent this problem, one may linearize equation (14), yielding [24]:

$$\Delta \mathbf{a}_i^T \Delta \mathbf{a}_{i-1} = \Delta l^2. \tag{15}$$

This method, known as the updated normal path method, results in a linear equation for the load increment. Equation (15) may be simplified by subtracting the constraint equation of the previous iteration. This gives

$$\Delta \mathbf{a}_{i-1}^T (\Delta \mathbf{a}_i - \Delta \mathbf{a}_{i-2}) = 0. \tag{16}$$

When we furthermore make the approximation

$$\delta \mathbf{a}_i \approx 2(\Delta \mathbf{a}_i - \Delta \mathbf{a}_{i-2}) \tag{17}$$

we obtain

$$\Delta \mathbf{a}_{i-1}^T \delta \mathbf{a}_i = 0. \tag{18}$$

Substituting equation (10) then gives, for $\Delta\mu_i$:

$$\Delta\mu_i = -\frac{\Delta \mathbf{a}_{i-1}^T \delta \mathbf{a}_i^{\mathrm{I}}}{\Delta \mathbf{a}_{i-1}^T \delta \mathbf{a}_i^{\mathrm{II}}}. \tag{19}$$

Both equations (14) and (15) have been employed very successfully within the realm of geometrically non-linear problems, where snapping and buckling of thin shells can be traced very elegantly. Nevertheless, for physically non-linear problems the method sometimes fails, which may be explained by considering that for physically non-linear problems, failure or bifurcation modes are often highly localized. Hence, only a few nodes contribute to the norm of displacement increments, and failure is not sensed accurately by such a global norm. As straightforward application of equations (14) or (15) is not always successful, we may amend these constraint equations by applying weights to the different degrees of freedom or omitting some of them from the constraint equation. The constraint equation (15) then changes into

$$\Delta \mathbf{u}_i^T \Delta \mathbf{u}_{i-1} = \Delta l^2, \tag{20}$$

where $\Delta \mathbf{u}_i$ contains only a limited number of the degrees of freedom of those of $\Delta \mathbf{a}_i$, and equation (19) changes in a similar manner. The disadvantage of modifying the constraint equation is that the constraint equation becomes problem dependent. As a consequence, the method loses some of its generality and elegance.

4. BIFURCATION ANALYSIS OF A BAR LOADED IN TENSION

We will now return to the problem of a perfect bar of elastic-softening material which is subjected to a uniformly distributed (tensile) load. From the preceding discussion it will be clear that the response of an imperfect bar in the post-failure regime will depend upon the number of elements and the degree of interpolation within the elements. For sake of simplicity, the latter variable is eliminated by electing four-noded elements with a bilinear displacement interpolation, so that we have a constant strain in the axial direction for each element. Then, the response in the post-peak regime only depends upon the number of elements.

When the bar is modeled by m elements, the limit point is an $m-1$ fold bifurcation point in the sense that $m-1$ alternative equilibrium branches emanate from this point apart from the fundamental mode which continues to deform homogeneously. The other bifurcation branches are associated with localization modes in one or more elements, whereby the other elements unload. This results in a fan of possible bifurcation branches which emanate from the bifurcation point. Which equilibrium path will be traversed depends on the number of elements in which the crack localizes (see Fig. 3).

When we introduce no imperfections, so that we do not transfer the bifurcation problem into a pure limit problem, a 64-bit processor is usually sufficient to guarantee that the bar deforms homogeneously also after the bifurcation point has been passed. Continuation on an equilibrium path which shows strain localization is then possible by adding a part of the eigenvector which corresponds to a zero eigenvalue to the fundamental solution (see the preceding section). In practice, a bifurcation point cannot be isolated exactly since we work with finite arithmetic. Consequently, we load the bar slightly, say 1%, beyond the bifurcation point and negative rather than zero eigenvalues are obtained. Nevertheless, this does not affect the essentials of the procedure.

In the example, we consider a material with a linear softening branch for which the ultimate strain ϵ_u at which the crack transfers no more normal stress, equals 10 times the strain at peak load. Let us first assume that the bar is modeled by only two elements in the axial direction (Fig. 4). The bar is loaded by a uniformly distributed traction slightly beyond the peak load, using indirect displacement control to overcome the limit point properly. Next, the tangent stiffness matrix is reformed and two negative eigenvalues are calculated; the corresponding eigenmodes having been plotted in Fig. 4. Adding a part of the latter eigenmode to the fundamental solution resulted in continuation on the localization path (A–C in Fig. 3). The resulting displacements when the load has become zero have been plotted in Fig. 5.

When we model the bar by more than two elements, we obtain a multiple bifurcation point. Indeed, we calculate m negative eigenvalues beyond peak load when we divide the bar into m elements. The selection of an appropriate eigenvector which gives localization in only one element then becomes a somewhat tedious task. The most simple way to solve this difficulty in practice, is to take the eigenvector corresponding to the lowest eigenvalue and add it to the fundamental solution. We will then converge on a localization branch which is not necessarily the lowest bifurcation branch. However, when we extract the lowest eigenvalue and the corresponding eigenvector for the new state and add them to the current displacement increment, we generally arrive at a lower bifurcation branch, whereby it seems superfluous to remark that an extremely small increment must be employed. Repeating this process several times finally results in convergence on the lowest bifurcation branch. For the present example, it implies that we finally converge on a branch in which the softening localizes in only one element while the other elements show unloading.

The above procedure is illustrated by an analysis in which the bar is divided in 10 elements. An eigenvalue analysis slightly beyond peak strength with a Jacobi-subspace method [23] resulted in 10 negative eigenvalues. The eigenvector belonging to the lowest eigenvalue has been plotted in Fig. 6. Adding this eigenvector to the fundamental mode did not result in localization in one element, but in five

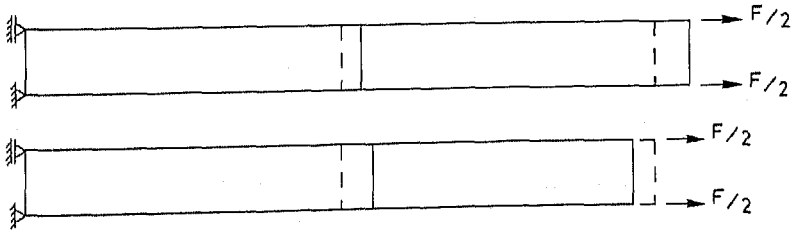

Fig. 4. Eigenmodes for two-element bar.

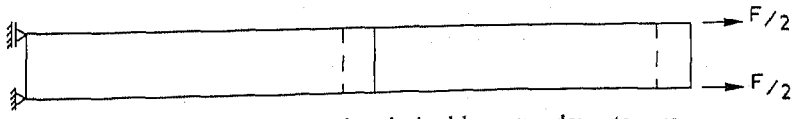

Fig. 5. Final displacements when the load has come down to zero.

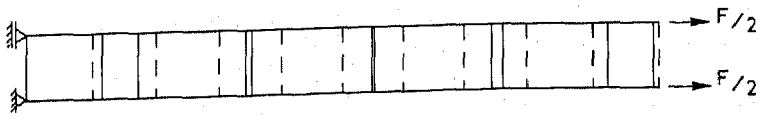

Fig. 6. Eigenvector for bar divided into 10 elements when all 10 elements show loading.

Fig. 7. Eigenvector for bar divided into 10 elements when five elements show loading and the other five show unloading.

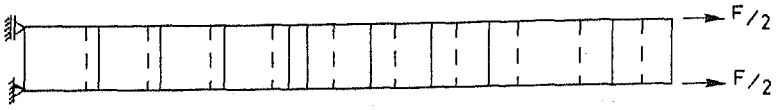

Fig. 8. Eigenvector for bar divided into 10 elements when three elements show loading.

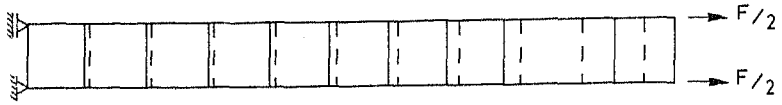

Fig. 9. Eigenvector for bar divided into 10 elements when only two elements still show loading.

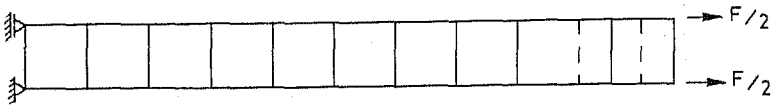

Fig. 10. Final displacements for bar composed of 10 elements showing localization in only one element.

elements, which is not surprising in view of Fig. 6. Performing an eigenvalue analysis for this tangent stiffness, in which the moduli of five elements are softening and the moduli of the remaining five elements unload via a secant branch [7–9, 26], resulted in five negative eigenvalues, the eigenvector corresponding to the lowest eigenvalue being plotted in Fig. 7. Adding this eigenvector to the current (small) displacement increment with localization in five elements resulted in a new equilibrium state with localization in three elements. A new eigenvalue analysis yielded three negative eigenvalues and addition of the eigenvector (Fig. 8) corresponding to the lowest eigenvalue to the current displacement increment resulted in localization in two elements. A final loop with the eigenvector of Fig. 9 yielded localization in one element (Fig. 10).

The case when the bar is modeled with 10 elements represents a critical case when the load falls down on the localization path without any additional displacement of the end of the bar (line A–D in Fig. 3), i.e. the strain increment in the element in which the deformation has localized together with the strain increments of the unloading elements is exactly zero. For a smaller number of elements the additional displacement at the end of the bar is positive, but for a greater number of elements, the additional displacement is negative, so that the total displacement at the end of the bar becomes *smaller* after the peak has been passed (line A–F in Fig. 3, which is for 20 elements). Obviously, such a "snap-back" behavior cannot be analyzed under direct displacement control, but only with indirect displacement control. Yet, many analysts have ignored the possibility of this phenomenon in the past, and many analyses have been terminated at such a point because of divergence of the iterative procedure. A further parallel can be drawn with experiments which cannot be performed properly under displacement control, e.g. with shear or other brittle failures. The observed explosive failure is then simply the result of an attempt to traverse an equilibrium path under improper static loading conditions.

5. MIXED-MODE FRACTURE IN A NOTCHED SPECIMEN

In the preceding section, it has been demonstrated how solutions can be obtained in the post-bifurcation regime. In the present section, we will show that the techniques and refinements discussed in the preceding sections also allow for tracing limit and post-limit behavior. Furthermore, we will show that some theses postulated in the preceding sections concerning the consequences of strain-softening are not merely academic, but that they are indeed encountered in concrete structures.

The first example which we consider, is the notched unreinforced beam of Fig. 11. The beam has been analyzed using eight-noded plane stress elements and six-noded triangles have been used in the transition region between the coarse part and the fine part of the mesh. Nine-point Gauss quadrature has been applied for the quadrilateral elements in order to prevent the occurrence of spurious zero-energy modes as much as possible [7]. The concrete has been modeled as linearly elastic in compression with a Young's modulus $E_c = 24800\ \mathrm{N/mm^2}$ and a Poisson's

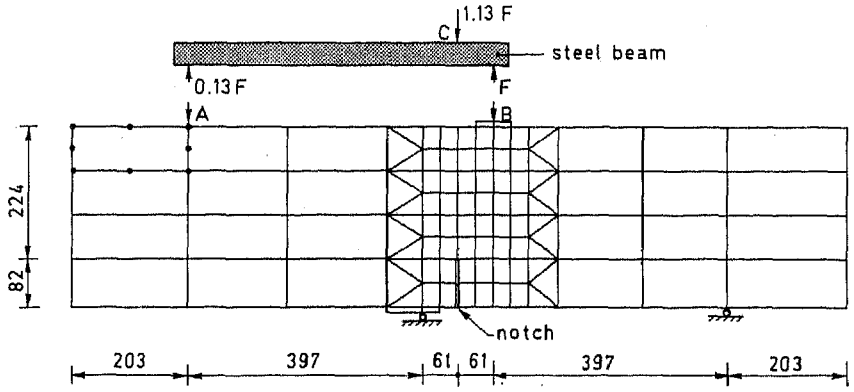

Fig. 11. Finite element mesh of notched beam.

ratio $\nu = 0.18$. This approach is justified in this case, because the compressive stresses remain low enough to avoid yielding in compression. In tension, the crack model as developed by de Borst [8, 9], de Borst and Nauta [7] and Rots *et al.* [26] has been employed. The crack parameters have been taken as: tensile strength $f_{ct} = 2.8$ N/mm^2 and fracture energy $G_f = 0.055$ N/mm. The width of the crack band was assumed to be $h = 10.167$ mm, and linear as well as nonlinear softening relations [10] have been employed.

Figure 11 also gives the loading configuration which shows that the beam is loaded asymmetrically so that the crack propagating from the notch shows opening as well as sliding. In the experiment [1] the load was applied cyclically to point C of the steel beam AB and was controlled by a feed-back mechanism with the so-called Crack Mouth Sliding Displacement (CMSD) as control parameter. After peak, the envelope of the load cycles falls down sharply (see Figs 12 and 13), which is particularly challenging for a numerical simulation.

A number of researchers have endeavored a numerical analysis of this beam [1, 5, 15, 17, 21, 26, 30], either with the smeared crack approach or with the discrete crack approach. Invariably, however, they adopted displacement control with respect to the point of load application (point C in Fig. 11) and all the calculated load–CMSD curves showed far too much ductility in the post-peak regime (Fig. 12). Moreover, the post-peak regime was repeatedly reported to be highly unstable and converged equilibrium states could not be obtained. Indeed, we will show that such attempts are deemed to fail.

In the present study, the loading process has been controlled indirectly by a displacement parameter and the results of Fig. 13 show that the computational results for the load–CMSD curves fall nicely within the experimental bounds, which is in sharp contrast with previous results. Initially, a global norm of displacements was employed, but this analysis was not successful as this constraint equation failed near peak load, probably for reasons as stated in the preceding discussion. Indeed, we observe a

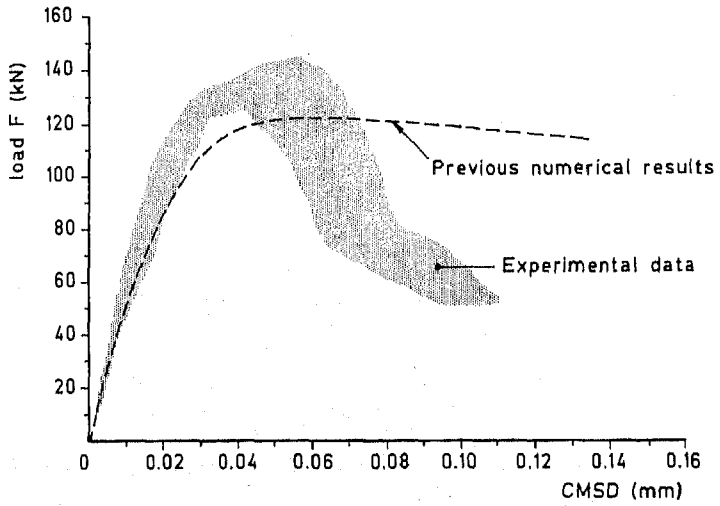

Fig. 12. Previous results for load vs CMSD. Computations performed with standard displacement control [26]. The shaded area denotes the range of experimental results.

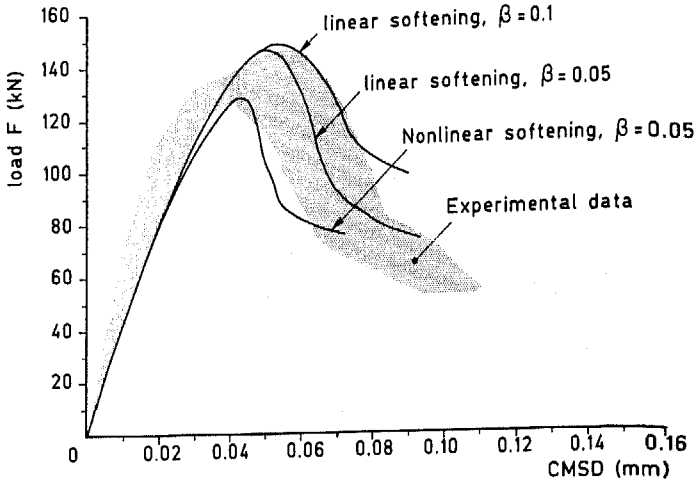

Fig. 13. Load vs CMSD computed with CMSD-control. The shaded area denotes the range of experimental results.

strong localization when we plot the eigen displacement mode at peak load (see Fig. 14). However, for the present problem, a displacement parameter which can be used to control the loading process is naturally available, namely the CMSD itself. In this way the numerical analysis entirely parallels the experiment. With CMSD-control, the load-increment is in the linearized version determined from the condition

$$\Delta u_i^T \Delta u_{i-1} = \Delta l^2, \tag{21}$$

with Δu_i the increment in CMSD in iteration i. Using the constraint eqn (21), the limit point could be overcome without problem with the same step size where the constraint formulae (14) and (15) failed.

Near peak load, an attempt to increment the load without CMSD control resulted in a divergence of the iterative procedure, but with CMSD-control and a full Newton–Raphson procedure a converged solution was obtained. Moreover, a negative pivot was encountered upon factorizing the tangent stiffness matrix after some iterations. An eigenvalue analysis was performed subsequently and this resulted in one negative eigenvalue with the eigenmode of Fig. 14 which is identical with the incremental displacement field at peak load. Hence, the peak load is a limit point and not a bifurcation point. After peak, the load was decremented and a genuine equilibrium path could be obtained.

If we assume that the beam of the test rig is infinitely stiff, we can calculate the vertical displacement of the point of load application C from the calculated diplacements of points A and B (Figs 15 and 16). For the analysis with nonlinear softening and a shear retention factor of 0.05, this results in the load–deflection curve of Fig. 17, which shows a violent snap-back behavior.

The snap-back after peak load entirely explains why previous solutions which adopted displacement control with respect to point C did not result in a stable post-peak response, as such a solution simply does not exist, at least not in the vicinity of the limit point. In fact, the situation is even worse when the analysis is performed under displacement control of point C. This is because the beam of the test rig cannot be modeled as infinitely stiff, so that after peak the elastically stored energy of this beam is partly released, thus making the snap-behavior even more violent.

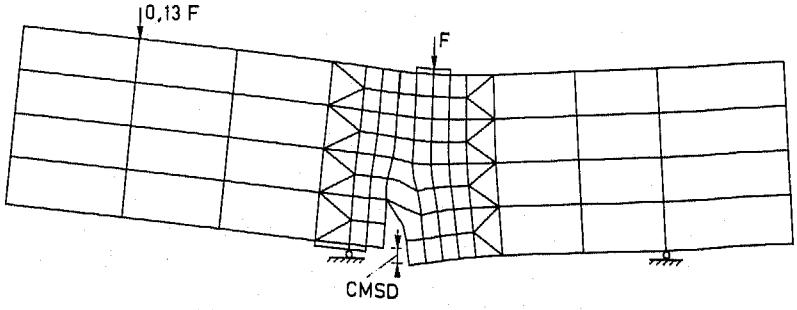

Fig. 14. Eigen-displacement field at peak load.

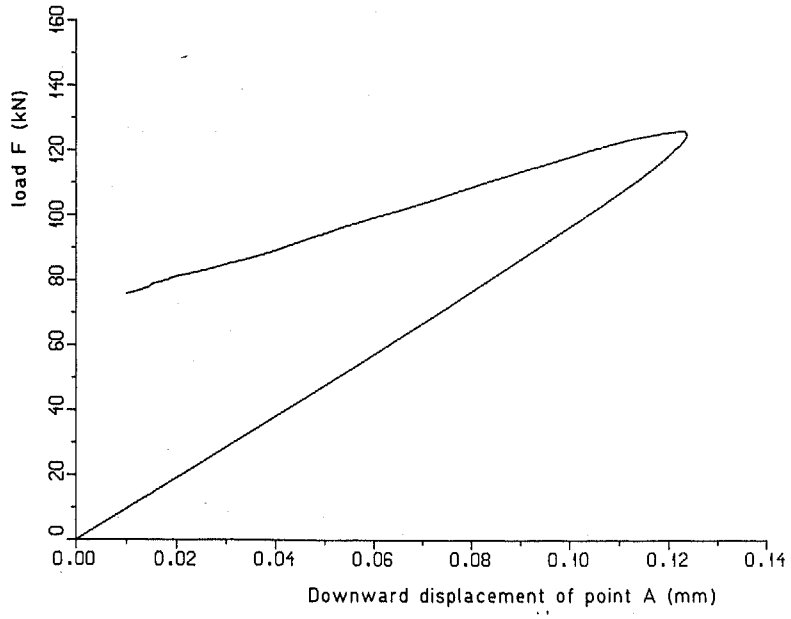

Fig. 15. Load–deflection curve of point A.

The load at point B versus the computed CMSD is plotted in Fig. 13. The most ductile curve corresponds to a shear retention factor $\beta = 0.1$ and a linear softening curve. We observe that the computed ultimate load overestimates the experimental values. Figure 18, which gives the incremental displacements and Figs 19 (a) and (b), which show the crack pattern at ultimate load, reveal that the crack arising from the notch has developed fully. Consequently, all stresses which are transferred in this crack are shear stresses, and these stresses cannot decrease because of the constant shear retention factor and because of the relatively high threshold angle for the formation of secondary cracks ($\alpha = 60°$ [7–9]). Indeed, beyond this point, the load again falls down sharply, which appeared to be due to formation of cracks elsewhere in the beam. Because the solution then becomes physically meaningless, this part of the curve has not been plotted.

At ultimate load, the beam is fully cracked and only shear stresses can be transferred across the cracks. As the magnitude of the shear stresses is

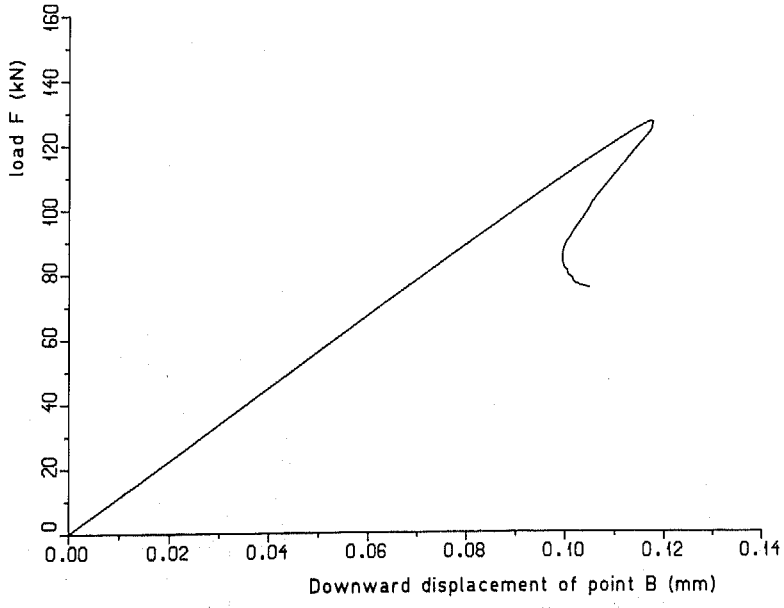

Fig. 16. Load–deflection curve of point B.

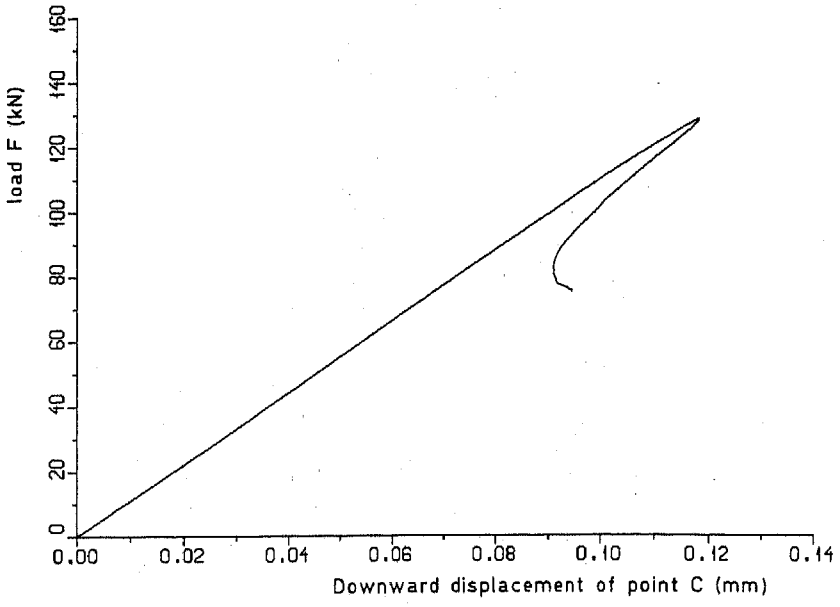

Fig. 17. Load–deflection curve of point C.

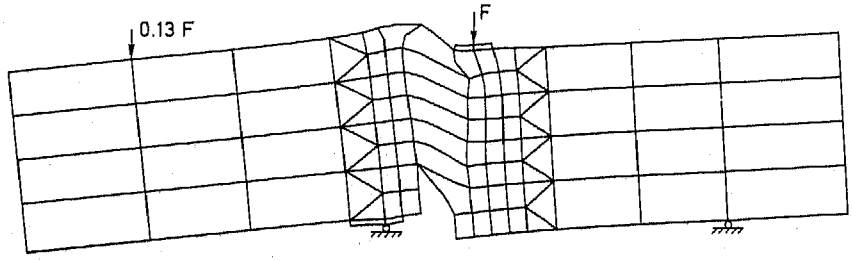

Fig. 18. Incremental displacements at ultimate load.

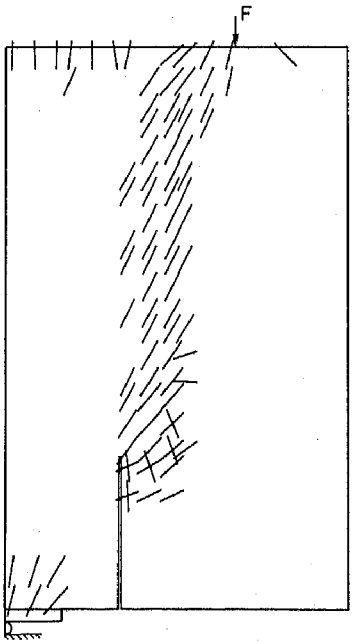

Fig. 19 (a). Crack pattern at ultimate load. All cracks.

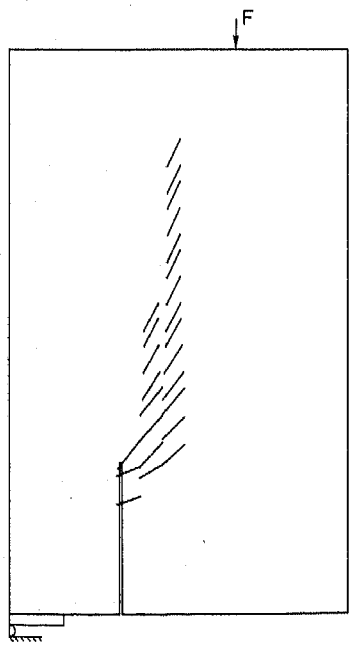

Fig. 19 (b). Crack pattern at ultimate load. Cracks which transfer no normal stress.

determined by the shear retention factor β, the ultimate load is primarily a function of β. The correctness of this hypothesis was confirmed in subsequent calculations with $\beta = 0.05$. These calculations were performed with a linear as well as with a non-linear softening curve and yielded a significantly lower ultimate load. It is interesting to note that use of a non-linear softening curve [10] instead of a linear softening curve yielded almost the same ultimate load (which strengthened the above hypothesis), but resulted in a significantly lower peak load. Hence, the shape of the softening curve also strongly influences the computational results [27].

6. TENSION-PULL SPECIMEN

It is a widespread belief that reinforcement stabilizes the numerical process. However, this is not generally true, as addition of reinforcement not only gives rise to stiffness differences in the structure, thus leading a deterioration of the condition of the stiffness matrix, but also adds to the possibility of the occurrence of spurious alternative equilibrium states and of snap-back behavior [13, 14]. We will demonstrate this by means of perhaps the most simple reinforced structure, namely an axisymmetric specimen with an axial reinforcing bar.

Specifically, we will consider the tension-pull specimen which is shown in Fig. 20 [16]. The reinforcing bar is given by the line AB and a linear bond–slip law is assumed between the concrete and the reinforcement, i.e. the relation between the slip and the shear stress between concrete and steel has been assumed to be linear. In fact, the element which is employed for the reinforcement is a combined steel-bond slip element [28]. The concrete has been modeled as linearly elastic in compression just as in the preceding example with a Young's modulus $E_c = 25000\ \mathrm{N/mm^2}$ and a Poisson's ratio $\nu = 0.2$. Also in this case the approach is justified because of the relatively low compressive stresses. The tensile strength has been assumed as $f_{ct} = 2.1\ \mathrm{N/mm^2}$ and a non-linear softening curve has been employed after crack formation with a fracture energy $G_f = 0.06\ \mathrm{N/mm}$. The shear retention factor β was taken equal to 0.1. The reinforcing bar was assigned a Young's modulus $E_s = 177000\ \mathrm{N/mm^2}$ and a yield strength $\sigma_y = 210\ \mathrm{N/mm^2}$.

The loading is applied to point A of Fig. 20 in the form of a concentrated load and the ensuing load–displacement diagram is given in Fig. 21. The present problem has much in common with the preceding example as also in this case straightforward application of a norm of incremental displacement to control the solution process did not work effectively. This can again be understood when we consider the incremental displacement fields just prior to and just beyond the limit point (Figs 22 and 23). Prior to the limit point, the elastic deformations of the bar are relatively so great, that they dominate the norm of incremental displacements. Just beyond the peak, when the crack near the centreline has localized, the incremental deformations of the reinforcing bar nearly vanish (they even change sign, so that we again have a snap-back) and the concrete is the prime contributor to the total norm of incremental displacements. However, because of the relatively great values of the steel deformations just prior to the limit point, the arc-length in the displacement space is not influenced significantly. In this case, the degrees of freedom belonging to the steel have therefore been omitted from the norm of incremental displacements for overcoming the limit point. For traversing the valley in the load–displacement curve of Fig. 21, on the other hand, the solution process has been controlled by the displacements of the steel, as then these displacements increase monotonically.

The present example is also well suited for assessing the question of whether an equilibrium state can be reached via a non-equilibrium path. It is the author's experience that this is often possible when we adopt standard displacement control and if there exists another equilibrium state which is located "not too far away" from the current state [9]. Indeed, when we attempted to analyze the present problem by prescribing the displacement of point A, we obtained a

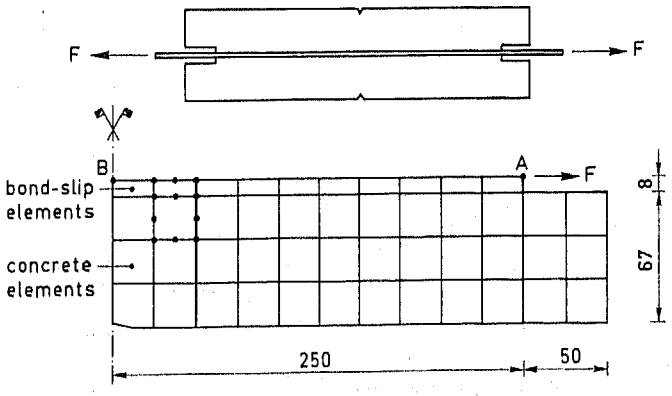

Fig. 20. Tension-pull specimen of Dörr [16].

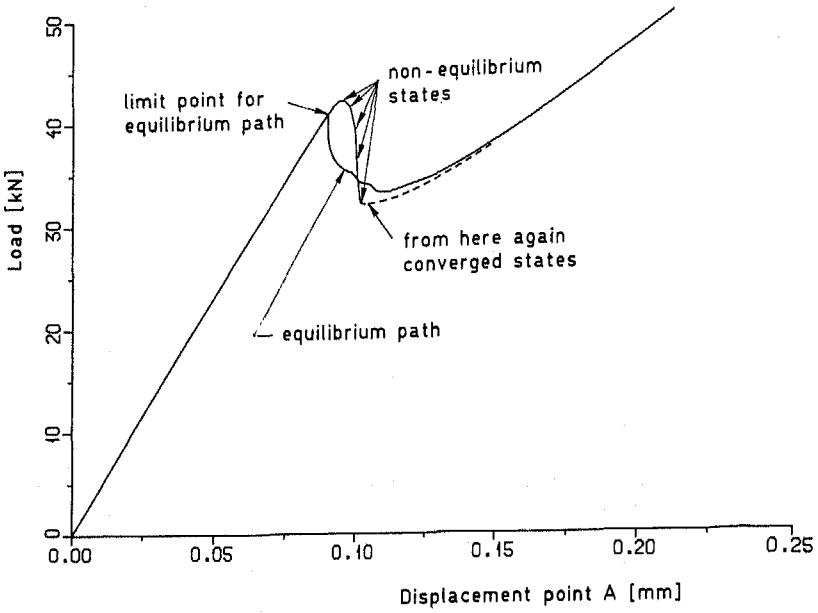

Fig. 21. Load vs displacement of the end of the bar.

number of non-converged states just after the limit point. This non-equilibrium path is indicated by the dotted line in Fig. 21. However, after the crack had localized, we again obtained converged equilibrium states (dashed line in Fig. 21), which indicated that we had arrived on a new equilibrium path. This illustrates that reaching another part of the equilibrium path via a number of non-equilibrium states is sometimes possible, provided that there exists a new equilibrium state which is "sufficiently close" to the previous equilibrium state. Here, the tension-pull specimen sharply contrasts with the previous example of mixed-mode crack propagation, as in the latter case equilibrium could not be restored using direct displacement control.

It is finally interesting to note that during the drop of the load no new cracks arise, so that the crack pattern of Fig. 24 remains unchanged. When the load is increased again, new "cone-shaped" cracks [18] arise which are a consequence of the reversal of the direction of the shear stresses along the bar near the centre of the specimen (see Fig. 25).

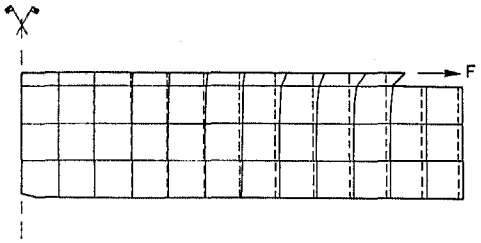

Fig. 22. Incremental displacement field just prior to the limit point.

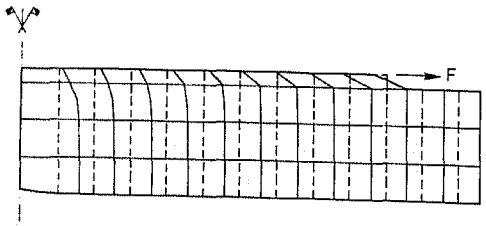

Fig. 23. Incremental displacement field just after the limit point.

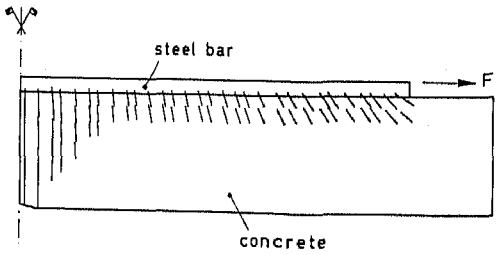

Fig. 24. Crack pattern at the first limit point.

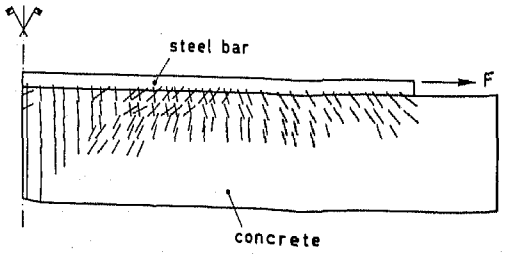

Fig. 25. Crack pattern at ultimate failure.

7. CONCLUSIONS

Use of strain-softening models may lead to snap-back behavior on a structural level. This observation, which has probably been made first by Crisfield [12], implies that structures composed of strain-softening material cannot always be analyzed using standard displacement control. The idea might arise that such snap-back behavior can be avoided by adapting the length of the softening branch to the element size as is being done in the fictitious crack model [20] or in the blunt crack band approach [4]. However, it has been shown by means of two concrete structures, a reinforced concrete structure and an unreinforced specimen, that this is not generally true, which is probably caused by the fact that the spread of the softening region is not known in advance.

As concrete structures cannot always be analyzed under standard displacement control, we have to resort to more sophisticated techniques. Here, the arc-length method seems a natural tool, but owing to the highly localized failure modes in strain-softening solids, the performance of this method is less than might be expected. A major improvement can be obtained when the global constraint equation is replaced by a constraint equation which employs only a limited number of degrees of freedom. As a consequence, the method, which is now perhaps better called "indirect displacement control", loses some of its elegance and generality.

A further problem with the use of strain-softening models is the non-uniqueness of solution. Numerical methods can locate bifurcation points by a combination of an incremental loading procedure and an eigenvalue analysis of the tangent stiffness matrix, while bifurcation in a discrete mechanical model can be forced by perturbing the fundamental solution by the eigenvector which belongs to the vanishing eigenvalue. It has been shown that this technique, which originates from geometrically nonlinear analysis, is also versatile for structures composed of strain-softening material.

Acknowledgements—The calculations reported in this paper have been performed with the DIANA finite element code on the VAX 11/780 computer of the Institute TNO for Building Materials and Structures. Major parts of the research reported in this paper have been assisted financially by CUR-Committee A 26 "Concrete Mechanics".

REFERENCES

1. M. Arrea and A. R. Ingraffea, Mixed-mode crack propagation in mortar and concrete. Report No. 81-13, Department of Structural Engineering, Cornell University, Ithaca, New York (1981).
2. K.-J. Bathe, *Finite Element Procedures in Engineering Analysis*. Prentice–Hall, Englewood Cliffs, NJ (1982).
3. Z. P. Bažant, Instability, ductility and size effect in strain-softening concrete. *ASCE J. Engng Mech. Div.* **102**, 331–344 (1976).
4. Z. P. Bažant and B. Oh, Crack band theory for fracture of concrete. *RILEM Mat. Struct.* **16**, 155–177 (1983).
5. J. Blaauwendraad, F. J. M. van den Berg and P. J. G. Merks, The use of the rough crack model of Walraven and the fictitious crack model of Hillerborg in F.E. analysis. In *Preprints William Prager Symp. on Mechanics of Geomaterials: Rocks, Concretes, Soils* (Edited by Z. P. Bažant), pp. 643–646. Northwestern University, Evanston, IL (1983).
6. R. de Borst, Application of advanced solution techniques to concrete cracking and non-associated plasticity. In *Numerical Methods for Non-linear Problems*, Vol. 2. (Edited by C. Taylor, E. Hinton, D. R. J. Owen and E. Onate), pp. 314–325. Pineridge Press, Swansea (1984).
7. R. de Borst and P. Nauta, Non-orthogonal cracks in a smeared finite element model. *Engng Comput.* **2**, 35–46 (1985).
8. R. de Borst, Computational aspects of smeared crack analysis. In *Constitutive Modelling of Concrete Structures*. Pineridge Press, Swansea (1986).
9. R. de Borst, Nonlinear analysis of frictional materials. Dissertation, Delft University of Technology, Delft (1986).
10. H. A. W. Cornelissen, D. A. Hordijk and H. W. Reinhardt, Experiments and theory for the application of fracture mechanics to normal and lightweight concrete. In *Preprints Int. Conf. on Fracture Mechanics of Concrete* (Edited by F. H. Wittmann). Elsevier, Amsterdam (1985).
11. M. A. Crisfield, A fast incremental/iterative procedure that handles snap-through. *Comput. Struct.* **13**, 55–62 (1981).
12. M. A. Crisfield, Local instabilities in the non-linear analysis of reinforced concrete beams and slabs. *Proc. Inst. Civ. Engrs* **73**, 135–145 (1982).
13. M. A. Crisfield, Difficulties of current numerical models for reinforced concrete and some tentative solutions. In *Proc. Int. Conf. Computer Aided Analysis and Design of Concrete Structures*, Part 1 (Edited by F. Damjanić, E. Hinton, D. R. J. Owen, N. Bicanić and V. Simović), pp. 331–358. Pineridge Press, Swansea (1984).
14. M. A. Crisfield, Some recent research on numerical techniques for structural analysis. In *Numerical Methods in Engineering: Theory & Applications*, Vol. 2 (Edited by J. Middleton and G. N. Pande), pp. 565–575. Balkema, Rotterdam (1985).
15. D. Darwin, Summary report: Bench-mark problems. In *Concrete Mechanics, Cooperative Research between Institutions in The Netherlands and the USA* (Edited by P. Gergely, R. N. White, J. W. Frénay and H. W. Reinhardt), pp. 66–80. Cornell University, Ithaca, New York (1984).
16. K. Dörr, Kraft- und Dehnungsverlauf von in Betonzylindern zentrisch einbetonierten Bewehrungsstaben under Querdruck. Forschungsbericht No. 30, Institute für Massivbau der Technischen Hochschule Darmstadt (1975).
17. R. Glemberg, Dynamic analysis of concrete structures. Publication 84:1, Department of Structural Mechanics, Chalmers Institute of Technology, Göteborg (1984).
18. Y. Goto, Cracks formed in concrete around deformed tension bars. *J. Am. Concrete Inst.* **68**, 244–251 (1971).
19. R. Hill, Some basic principles in the mechanics of solids without a natural time. *J. Mech. Phys. Solids* **7**, 209–225 (1959).
20. A. Hillerborg, M. Modeer and P. E. Petersson, Analysis of crack formation and crack growth in concreate by means of fracture mechanics and finite elements. *Cement Concrete Res.* **6**, 773–782 (1976).
21. L. Nilsson and M. Oldenburg, On the numerical simulation of tensile fracture. In *Preprints Europe-US Symposium on Finite Element Methods for Non-linear Problems* (Edited by P. G. Bergan, K.-J. Bathe and W. Wunderlich), paper I.4. Norwegian Institute of Technology, Trondheim (1985).

22. S. Pietruszczak and Z. Mróz, Finite element analysis of deformation of strain softening materials. *Int. J. Numer. Meth. Engng* **17**, 327–334 (1981).
23. A. Ralston and P. Rabinowitz, *A First Course in Numerical Analysis*, 2nd edn. McGraw–Hill, Tokyo (1978).
24. E. Ramm, Strategies for tracing the nonlinear response near limit points. In *Nonlinear Finite Element Analysis in Structural Mechanics* (Edited by W. Wunderlich, E. Stein and K.-J. Bathe), pp. 63–83. Springer, Berlin (1981).
25. E. Riks, An incremental approach to the solution of snapping and buckling problems. *Int. J. Solids Struct.* **15**, 529–551 (1979).
26. J. G. Rots, P. Nauta, G. M. A. Kusters and J. Blaauwendraad, Smeared crack approach and fracture localization in concrete. *Heron* **30**, 1–48 (1985).
27. J. G. Rots, Strain-softening analysis of concrete fracture specimens. In *Preprints Int. Conf. on Fracture Mechanics of Concrete* (Edited by F. H. Wittmann), pp. 115–126. Elsevier, Amsterdam (1985).
28. J. G. Rots, Bond–slip simulations using smeared cracks and/or interface elements. Research report, Structural Mechanics Group, Department of Civil Engineering, Delft University of Technology (1985).
29. H. L. Schreyer and Z. Chen, The effect of localization on the softening behavior of structural members. In *Constitutive Equations: Macro and Computational Aspects* (Edited by K. J. Willam), pp. 193–204. *ASME* (1984).
30. K. J. Willam, Computational aspects of concrete mechanics. In *Concrete Mechanics, Cooperative Research between Institutions in The Netherlands and the USA* (Edited by P. Gergely, R. N. White, J. W. Frénay and H. W. Reinhardt), pp. 81–109. Cornell University, Ithaca (1984).
31. K. J. Willam, Experimental and computational aspects of concrete fracture. In *Proc. Int. Conf. Computer Aided Analysis and Design of Concrete Structures*, Part 1 (Edited by F. Damjanić, E. Hinton, D. R. J. Owen, N. Bicanić and V. Simović), pp. 33–70. Pineridge Press, Swansea (1984).